

Sequential Printing by Laser-Induced Forward Transfer To Fabricate a Polymer Light-Emitting Diode Pixel

James R. H. Shaw-Stewart,^{*,†,‡,§} Thomas K. Lippert,^{*,‡} Matthias Nagel,[†] Frank A. Nüesch,^{*,†,§} and Alexander Wokaun[‡]

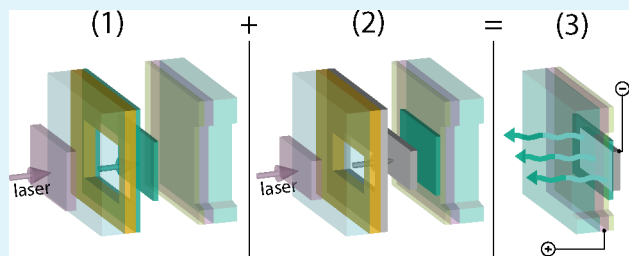
[†]Laboratory for Functional Polymers, EMPA Swiss Federal Laboratories for Materials Science and Technology, Überlandstrasse 129, CH-8600 Dübendorf, Switzerland

[‡]General Energy Research Department, Paul Scherrer Institut, CH-5232 Villigen-PSI, Switzerland

[§]Section de Science Et Génie des Matériaux, EPFL, CH-1015, Lausanne, Switzerland

ABSTRACT: Patterned deposition of polymer light-emitting diode (PLED) pixels is a challenge for electronic display applications. PLEDs have additional problems requiring solvent orthogonality of different materials in adjacent layers. We present the fabrication of a PLED pixel by the sequential deposition of two different layers with laser-induced forward transfer (LIFT), a “dry” deposition technique. This novel use of LIFT has been compared to “normal” LIFT, where all the layers are transferred in a single step, and a conventional PLED fabrication process. For the sequential LIFT, a 50-nm film of an alcohol-soluble polyfluorene (PFN) is transferred onto a receiver with a transparent anode, before an aluminum cathode is transferred on top. Both steps use a triazene polymer dynamic release layer and are performed in a medium vacuum (1 mbar) across a 15 μm gap. The rough morphologies of the single-layer PFN pixels and the PLED device characteristics have been investigated and compared to both bilayer Al/PFN pixels fabricated by normal LIFT and conventionally fabricated devices. The functionality of the sequential LIFT pixels (0.003 cd/A, up to 200 mA/cm², at 30–40 V) demonstrates the suitability of LIFT for sequential patterned printing of different thin-film layers.

KEYWORDS: sequential laser deposition, LIFT, triazene polymer, PLED pixels, thin-films, patterned deposition, laser direct-write, OLEDs



INTRODUCTION

Organic light-emitting diodes (OLEDs) have been investigated in detail for nearly a quarter of a century,¹ but improved OLED deposition techniques are still required to become a commercially competitive display technology, particularly for solution-processable polymeric materials in polymeric OLEDs (PLEDs). Laser-induced forward transfer (LIFT) is a technique that was also developed around 25 years ago,² and has seen heightened interest in recent years, but is still very much in the developmental stages.³ From the first simple single-layer transfers, an early improvement was the addition of a “sacrificial” layer, to aid the propulsion of the material of interest. This intermediate layer, known as a dynamic release layer (DRL),⁴ allows the transfer of materials that cannot absorb the laser light, or are too sensitive to the light.

Our group has pioneered the use of a triazene polymer (TP) DRL, and TP DRL-based LIFT has since been used to successfully transfer numerous materials including biological cells,⁵ quantum dots,⁶ organic thin-film transistors,⁷ ceramics,⁸ polystyrene microbeads,⁹ polymeric sensors,¹⁰ and liposomes.¹¹ The first successful transfers of PLED materials for functional devices were achieved with a TP DRL.¹² Subsequently, a modified LIFT technique has been applied to transfer the

functional layer as a solution,¹³ and the original DRL-LIFT technique has successfully transferred (LIFTed) more-complex multilayer PLED architectures.^{14,15} A big limitation for multilayer stacks of solution-processable materials is solvent compatibility, which has been addressed by chemical modification of the materials, such as to make nonpolar compounds polar,¹⁶ but is still not applicable to all materials. One of the potential advantages of LIFT is to transfer otherwise incompatible layers on top of one another.

Here, we present sequential printing by LIFT (“sequential LIFT”) of, first, the light-emitting polymer (LEP) layer onto the receiver with the transparent anode, followed by the metal cathode, to fabricate functioning PLEDs. Previously, all OLEDs fabricated by LIFT have been made either by putting the cathode and active materials together as a stack on the donor substrate (“normal LIFT”),^{12,14,15} or by evaporating the cathode on afterward.¹³ The transfers take place at a reduced pressure of 1 mbar, with a spacer between the donor substrate, determined by optimizing the LIFT process.¹⁷ Multilayer,

Received: April 6, 2012

Accepted: June 27, 2012

Published: June 27, 2012

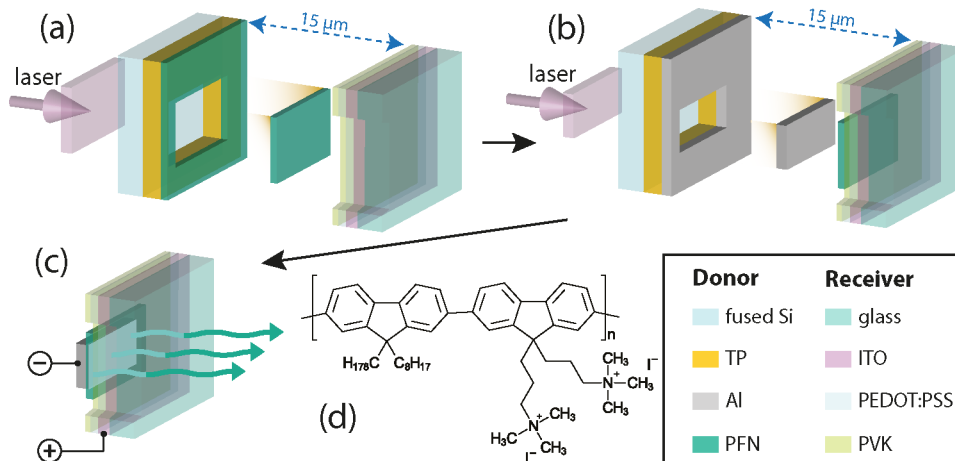


Figure 1. Scheme showing the transfer outlined in this paper with huge horizontal exaggeration (thickness of films and gap width): (a) deposition of the PFN on the glass/ITO/PEDOT:PSS/PVK receiver substrate; (b) deposition of the Al on top of the PFN; (c) final PLED with a bias applied; and (d) chemical structure of PFN.

three-color PLED pixels have already been deposited successfully using optimized normal LIFT, where different cathode/organic material stacks were deposited side by side.¹⁵

A schematic of the sequential LIFT process is shown in Figure 1, demonstrating two separate deposition steps (Figures 1a and 1b) and the final pixel operation (Figure 1c). The donor substrate is shown on the left and the receiver on the right for panels a and b in Figure 1, and Figure 1c shows the final receiver substrate with a bias applied across the device. The material used is PFN (poly[(9,9-di(3,3'-N,N'-trimethyl ammonium) propyl fluorenyl-2,7-diyl)-alt-(9,9-dioctyl fluorenyl-2,7-diyl)]). PFN is a standard polymeric OLED material, well-studied in the literature, but normally used as an electron-injecting layer or a host for phosphorescent dopants.^{16,18,19} PFN is particularly useful for sequential LIFT, because it is soluble in methanol, which does not dissolve most of the other polymeric films soluble in other organic solvents. This means that it can be spin-coated directly on top of TP, enabling the transfer of single PFN films, as demonstrated in this article.

EXPERIMENTAL SECTION

Substrate Preparation. The LIFT donor substrates use UV-transparent fused-silica slides (25 mm × 25 mm × 1 mm), cleaned thoroughly with solvent and detergent baths, and UV ozone treatment. The fused-silica substrates were spin-coated at 1500 rpm with 3 wt % solutions of TP (TP-6a in ref 20). Profilometry shows that this gives a thin film thickness of 190 ± 10 nm. The PFN was used as bought from ADS (American Dye Source, Inc.), and the structure is shown in Figure 1d. A solution was made of PFN in methanol:DMF (99:1) and spin-coated on top of the insoluble TP film to make a ~50 nm film with a root-mean-square (rms) roughness of ~3 nm. The cathode donor substrates were made by thermally evaporating 80 nm films of aluminum onto the TP films at pressures below 1×10^{-5} mbar, with the thickness measured using a quartz-crystal microbalance.

The LIFT receiver substrates use prepatterned 140 nm thick ITO (indium-doped tin oxide) glass slides (25.4 mm × 25.4 mm × 1 mm). These were spin-coated with two hole-transporting layers (HTLs): 60 nm PEDOT:PSS (poly[3,4-ethylene dioxythiophene] blended with poly[styrene sulfonate], Clevios P Al4083), and 40 nm of PVK (poly[N-vinyl carbazole], Sigma-Aldrich).

Conventionally fabricated devices were exactly the same as LIFT receiver substrates, but with the PFN and cathode deposited directly on top of the PVK. An ~50 nm thick film of PFN was deposited by spin-coating, before a patterned ~50 nm thick film of Al was evaporated on top.

The spin coating of the PFN was slightly problematic, because it is not very soluble in methanol, so a small amount of DMF was added as suggested by the suppliers (ADS). The spin-coated films exhibited a periodic undulation observable by optical microscopy, seen in Figure

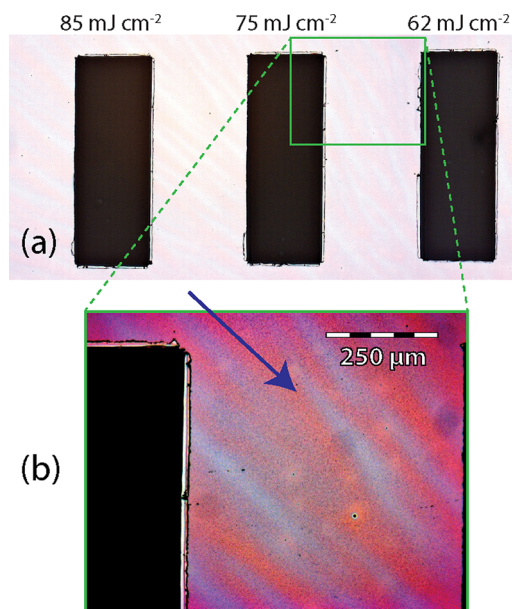


Figure 2. PFN donor substrate for the pixels on the receiver substrate in Figure 3, showing (a) dark ablation craters from various laser fluences and (b) a closeup on the gap between the 75 and 62 mJ/cm² ablation craters, with the contrast increased to show the periodic pattern more clearly.

2. These sort of effects have been observed before, particularly in the case of polymer bilayers (i.e., both the LIFT donor, TP/PFN, and the conventional device, PVK/PFN), and the authors suggest modifications to the spin-coating process to suppress this long-range surface roughness.²¹

LIFT Setup. The receiver substrate was placed opposite the donor substrate separated by a steel spacer, which gave a gap width of ~15 μm from interferometry.¹⁷ The substrates with the spacer are shown in Figures 1a and 1b, and were placed in a vacuum chamber where a dry roughing pump reduced the pressure to 1 mbar. Single pulses from a XeCl excimer laser ($\lambda = 308$ nm, $\tau = 30$ ns) were used for the ablation

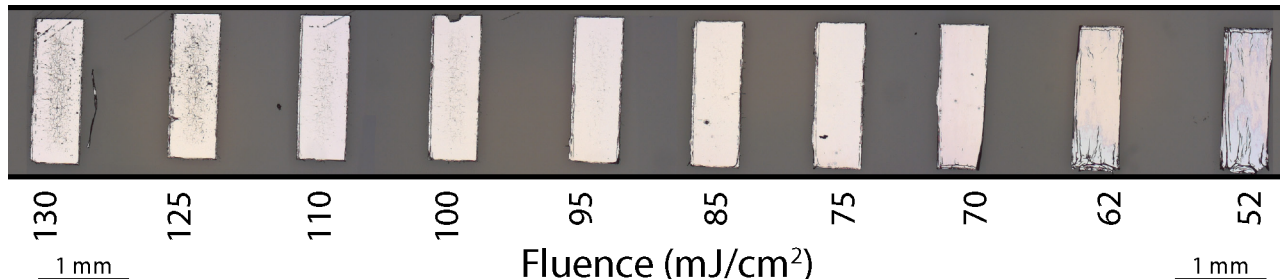


Figure 3. PFN pixels printed from the LIFT donor substrate shown in Figure 2, using the normal LIFT process for a variety of fluences from 130 mJ/cm^2 to 52 mJ/cm^2 .

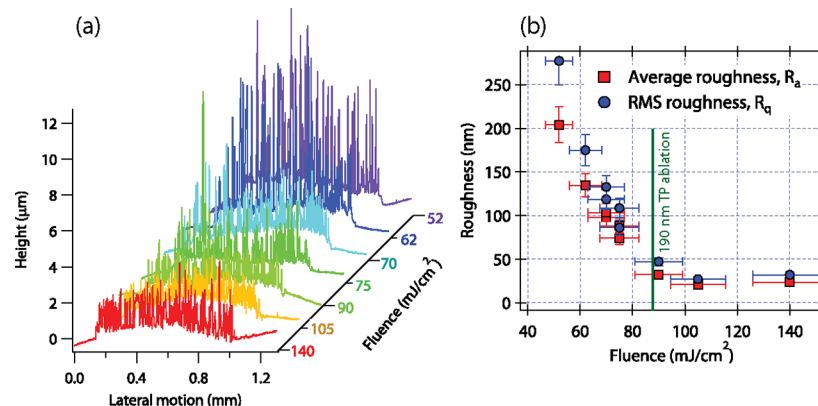


Figure 4. Surface roughness of PFN pixels transferred at different fluences from a donor substrate of 190 nm TP/50 nm PFN: (a) surface profiles, which were used to calculate (b) the roughness values. The green line indicates the fluence ($\sim 90 \text{ mJ/cm}^2$) required for frontside ablation of 190 nm TP.²²

of the TP DRL. Deliberately larger PFN pixels, with a width of $\sim 700 \mu\text{m}$, were transferred before the Al pixels with a width of $\sim 500 \mu\text{m}$, in order to prevent the Al from short-circuiting the PFN. The rectangular pixel size was controlled by projection through a mask, followed by imaging onto the TP using a lens with a 4-fold demagnification. The LIFT procedure, including the details of the laser setup and optimization of the gap width and environmental pressure for the LIFT process, are explained in detail elsewhere.¹⁷ To summarize, the architecture of all the devices made in this study is ITO/PEDOT:PSS/PVK/PFN/Al.

Device Characterization. A Keithley Model 2400 sourcemeter was used to apply a bias across the devices, as shown in Figure 1c, and measure the current–voltage (I – V) characteristics. A Minolta Model LS-110 light meter was linked to the sourcemeter by a home-built labview program to allow synchronous luminance measurements, and the process has been outlined in detail previously.¹⁴

Fluorescence measurements were taken using a Jobin Yvon Horiba Model FL311 Fluorolog. All electroluminescence (EL) spectra were obtained using an external arrangement with optic fibers. The photoluminescence (PL) spectra were made externally, in the same way as the EL spectra, and with a solution inside the apparatus. The pixels were examined using standard light microscopes (Leica Model DM2000 and Zeiss Model Axiovert), and profilometry measurements were taken using an Ambios XP-1 system.

RESULTS AND DISCUSSION

The results are presented in two sections: pixel fabrication and device characterization. Pixel fabrication focuses on the LIFT of pixels using two different types of LIFT, both with optimized substrate gap and reduced pressure conditions.¹⁷ “Sequential LIFT” refers to the LIFT of the functional EL layer and the cathode layer separately, as shown schematically in Figure 1. “Normal LIFT” refers to the LIFT of a stack of both the cathode and the functional electroluminescent (EL) layer,

already established for the fabrication of PLEDs.^{14,17,22} The device characterization looks at the functionality of the pixels fabricated using the processes in the previous section, and compares them to the “conventionally fabricated devices”.

Pixel Fabrication by LIFT. Normal LIFT. The normal LIFTed pixels made with PFN have a morphology as good as those done with another polyfluorene (PFO),¹⁵ despite the PFN being spin-coating from a different solvent (methanol) to the PFO (toluene:*p*-xylene), and appearing to form slightly undulated PFN films (see the periodic undulation on the PFN film on the donor substrate in Figure 2). Transferred pixels are shown in Figure 3. Pixels with device characteristics very similar to conventional devices were fabricated by LIFT in this normal way.

The PFN/Al pixels are shown in Figure 3 for different LIFT laser fluences from 52 mJ/cm^2 to 130 mJ/cm^2 . Over this large range of fluences, the pixels are remarkably homogeneous in terms of larger-scale features visible in Figure 3. This shows that the LIFT process is very accommodating for small deviations in the laser fluence. The metal/organic bilayer pixel structure of normal LIFT creates pixels with much smoother morphologies than the pixels created for sequential LIFT.

Sequential LIFT. The optimal fluence for the transfer of 80 nm Al/50 nm polyfluorene bilayers has previously been determined to be $\sim 75 \text{ mJ/cm}^2$,¹⁷ and this was the fluence ($\pm 10 \text{ mJ/cm}^2$) used for the transfers of both layers of the functional OLED pixels in this study. The PFN film was LIFTed fairly successfully over quite a wide range of fluences, but Figure 4 shows how the PFN surface roughness increases as the fluence decreases. The PFN film on the donor substrate,

before LIFT, is very smooth, with a roughness of <4 nm, substantially lower than the transferred values in Figure 4b.

The optical micrographs in Figure 5 show the nature of the roughness, with a mosaic pattern that increases as the fluence

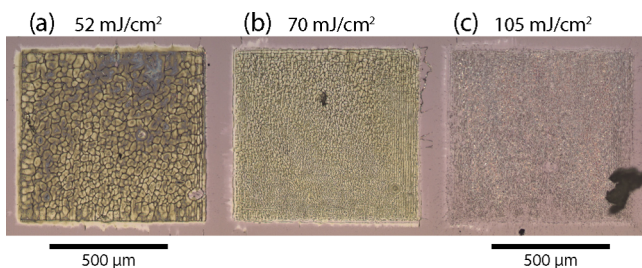


Figure 5. Light micrographs of single-layer PFN pixels transferred at (a) 52, (b) 70, and (c) 105 mJ/cm^2 .

decreases. Below 50 mJ/cm^2 and above 140 mJ/cm^2 , effectively no transfer was observed. The pixel from LIFT at 52 mJ/cm^2 , Figure 5a, shows a dark yellow and purple coloration which decreases in intensity at the higher fluence transfers (see Figures 5b and 5c). In combination, there is a mosaic pattern, the outline of which probably provides the ridges which contribute to the large surface roughness in Figure 4. The mosaic pattern becomes finer as the fluence increases. The combination of the color differences and the coarse mosaic structure points toward distortion of the film in the transfer process.

To understand these observations, possible differences between the transfers at different fluences need to be considered. First, more TP will be ablated at higher fluences. In fact, $\sim 80 \text{ mJ}/\text{cm}^2$ is required to fully ablate 190 nm TP in the “frontside” ablation configuration,²³ meaning that some TP should remain unablated on the pixel for the transfers at 52 and 70 mJ/cm^2 (see Figures 5a and 5b). In addition to the greater ablation depth of the TP, the thermal buildup in the PFN layer will be higher at higher fluences, and the flyer (flyer = pixel when being transferred) will also travel faster across the gap at higher fluences.²⁴

The difference between TP ablation depths is probably the best explanation for the different interference colors of the PFN pixels in the micrographs in Figure 5, but the mosaic pattern is not easily explained by variable triazene polymer ablation depths. Nevertheless, similar observations have been made from triazene ablation, first in shadowgraphy of single-layer TP films, where the flyers showed clear morphological distortion,²⁴ and second in the microscopy of transferred polymeric pixels “in contact”, where similar pixel surface roughness was observed for both single-layer TP films²³ and gelatin films with a TP DRL.²⁵ The mechanism behind these morphological distortions is not yet understood, but is probably derived from a thermal and/or a mechanical origin.¹⁷

Early research into triazene surface modification by UV laser modification shows a remarkably similar pattern to the mosaic pattern in Figure 5a.²⁶ In their results, the boundaries were troughs rather than peaks, therefore termed “volcano” structures, and the consequence of 250 pulses of 36 mJ/cm^2 with 248 nm irradiation. This is obviously a very different mechanism of formation, but the similarity between the patterns points toward a common laser-based origin.

Pixel Fabrication Discussion. Comparing the normal LIFT technique to the sequential LIFT technique deserves

further discussion. Previously, it has been hypothesized that the polymeric layer stabilizes the metal layer,²⁷ but the idea that the metal layer stabilizes the polymer is less obvious. Nevertheless, the difference between the normal LIFTed pixels in Figure 3 and the single-layer PFN pixels in Figure 5 is very clear. The roughness of the single-layer PFN pixels is also remarkable, with peak heights reaching over 10 μm . In addition, it is interesting that the PFN pixel roughness appears to level off at approximately the fluence where all the TP should have been ablated by frontside ablation of $\sim 90 \text{ mJ}/\text{cm}^2$.

In Figure 2, periodic undulation of PFN films on the donor substrate was observed. Despite this long-range periodicity, the PFN films formed by spin-coating are very smooth. When the PFN/Al pixels are fabricated by normal LIFT in Figure 3, the films are still very smooth, but the single-layer PFN pixels in Figures 4 and 5 are extremely rough. The main difference between the normal and sequentially LIFTed PFN pixels is the absence of aluminum in the single-layer PFN pixels, in Figure 5. The explanation for the high roughness of the single-layer PFN pixels must revolve around the absence of the aluminum. The absence of a metal layer could allow the gaseous decomposition products of TP ablation to penetrate, or at least punch into, the soft PFN film.

The PFN must undergo fairly extensive plastic deformation during LIFT to create the roughness seen in Figure 4 without ripping. The stresses that create this plastic deformation may usually be accommodated by the brittle metal film as elastic strain in normal LIFT. The only visible strain of a brittle film would be cracks when the stress is high enough; however, the bilayer of PFN and Al may help to dissipate some stress in small-scale plastic deformation of the PFN while the Al layer remains complete. This may explain why the bilayer pixels in Figure 3 have morphologies that are much better than those in Figure 5.

Device Characterization. Conventional Devices. The device characteristics of conventionally fabricated devices, alongside normal LIFTed pixels, with the architecture PEDOT:PSS/PVK/PFN/Al are shown in Figure 6. There are two conventionally fabricated device plots, a first run up to 100 mA/cm^2 , and then a second run of the same device. The difference is most stark in Figure 6b, where the luminance of the conventional device on the first run is shown to remain below 5 cd/m^2 all the way up to 100 mA/cm^2 , whereas it starts to rise dramatically above 20 mA/cm^2 on the second run, and this difference in luminance is reflected in the efficiency rise on the second run. The external quantum efficiency is over an order of magnitude higher on the second run than the first run.

A second observation is shown in the micrograph inset identified as Figure 6c, where the electroluminescence can be seen directly. There are distinct striations running diagonally through the device, highlighted by white arrows. They look like ripples with peaks and troughs of light-outcoupling. They appear to be permanent features in the PFN films, but are hard to identify when the device is not in operation, except when the device is burnt through (see Figure 6d). This indicates that the brightness peaks probably do correspond to where the majority of the current is passing through the device, as that would then burn-in the pattern after overloading the device. The conventional PFN device exhibits decent performance as long as the voltage stays well below 20 V. At current densities only just above 100 mA/cm^2 , the burnout begins, therefore luminances above 80 cd/m^2 are hard to reach. At that point,

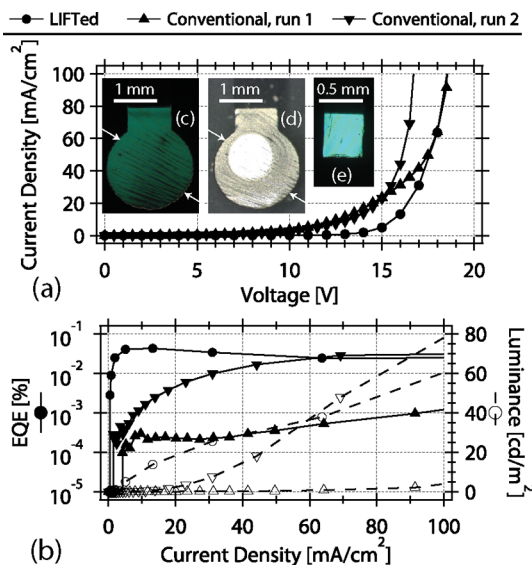


Figure 6. Device characteristics for both the conventionally fabricated device and the normal LIFTed PFN pixel are shown. (a) Current density plotted against voltage, and (b) external quantum efficiency (EQE) and luminance both plotted against current density. Micrographs of a conventional device (c) during operation and (d) after burnout, and (e) a LIFTed pixel during operation are shown as insets.

the device burns out, leaving the white product shown in Figure 6d.

Compared to literature values, these devices exhibit comparable performance (on the second run).¹⁶ The EQE for PVK/PFN/Al reported in ref 16 was 0.09%, which is not far above the 0.03% in this study. However, that article was the first report on this class of ionic, alcohol-soluble polyfluorenes and (a) they used a different anion (Br^- instead of I^- used in this study), (b) they synthesized the compounds themselves, guaranteeing their purity, and (c) the PL (and to a more minor extent, the EL) thin-film spectra were slightly different from that presented in Figure 7, but the solution PL spectra are fairly similar.¹⁶

Normal LIFTed Pixels. The device characteristics in Figure 6 show that the normal LIFTed pixels demonstrate very similar performance to the conventionally fabricated device, and actually performs more efficiently on the first run. The burnout voltages and current densities are also the same, and the ripples observed in the conventional devices can also be seen in the LIFTed pixels. However, as the ripples are only a fairly large scale ($\sim 100 \mu\text{m}$), they are not as obvious; however, in Figure 8c, they can be seen running parallel to the pink arrow at the top of the pixel.

Some minor pixel morphological features have been highlighted in Figure 8 to compare with the sequentially LIFTed pixel. The green arrows highlight a spot defect that grows upon operation, and the white arrow shows a linear defect which seems to be completely benign upon operation. These results suggest that the linear features are probably generally folds, whereas the spots are probably holes that grow because of the high current density burning the material. There is no evidence of the cracks observed for transfers at atmospheric pressure,^{12,14} and the folds and spots are fairly minimal as seen before,¹⁵ and could probably be removed by optimizing the entire fabrication process to further minimize the chances of heterogeneity and contamination of the samples.

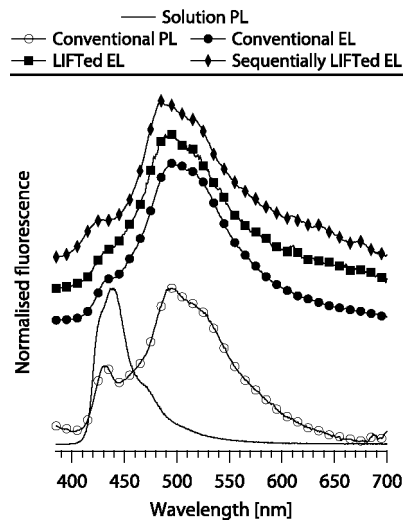


Figure 7. Comparison between the LIFTed pixels and conventionally fabricated device electroluminescence (EL) spectra. The photoluminescence (PL) spectra of the PFN methanol solution, and the conventionally fabricated device are also shown.

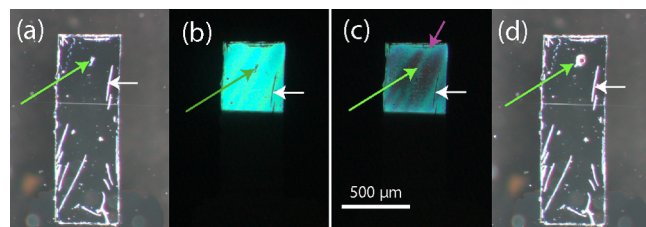


Figure 8. Optical micrographs of a LIFTed PFN pixel, from an Al/PFN stacked donor substrate (a) before, (b, c) during, and (d) after operation. The green arrow points out an existing defect that grows upon operation, and the white arrows point out a fold that does not grow.

Sequential LIFTed Pixels. A functional sequentially LIFTed pixel is shown in Figure 9, with the corresponding

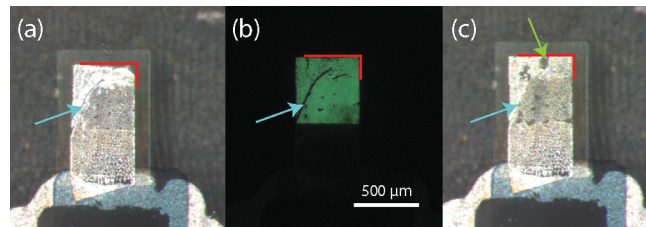


Figure 9. Optical micrographs of a sequentially transferred PFN PLED (a) before, (b) during, and (c) after operation. The red lines highlight a corner “smoothed out” by the operation, the blue arrow is pointing out a permanent fold, and the green arrow shows an example of where the device has burned through by overloading during operation.

device characteristics outlined in Figure 10. Figure 9 shows optical micrographs of a sequentially LIFTed pixel before operation (Figure 9a), during operation (Figure 9b), and after operation (Figure 9c). The differences between Figures 9a and 9b show that the pixel morphology changes quite significantly upon operation. The first observation is that the smaller ripples and folds (e.g., the top right-hand corner of the pixel, highlighted with a red corner in Figure 9) are smoothed out,

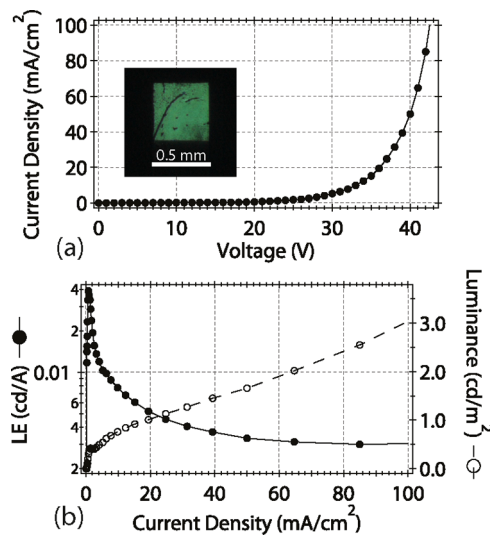


Figure 10. Device characteristics for sequentially transferred PFN PLED pixels are shown: (a) current density versus voltage with an optical micrograph of a pixel under operation in an inset, and (b) luminous efficiency (LE) and luminance versus current density.

but the big ones (e.g., the arc down the left of the pixel, shown by a blue arrow) are retained and emit no light. When a high bias is applied, burnout of the aluminum cathode begins, and holes are formed such as that highlighted with a green arrow in Figure 9c.

Figure 10a shows the diodic behavior of the device. The device shows good current density–voltage diode characteristics, with a distinct turn-on voltage of ~ 30 V. The luminance and luminous efficiency (LE) are presented in Figure 10b, as a function of current density. The device efficiency shows a large fall from a low current-density value of above 0.02 cd/A to a stable value of ~ 0.003 cd/A. This is not as good as the multilayer normal LIFTed pixels in Figure 6, but comparable to previous multilayer transfers of MEH-PPV.^{12,14} The electroluminescence in Figure 9b shows the blue-green nature of the emission, matching the EL spectra in Figure 7, and the original EL spectra from the literature.¹⁶

The high operating voltage of the sequentially LIFTed pixel could easily be attributed to porosity in the PFN film, which is indicated by the large thickness and roughness of the transferred PFN films in Figure 4. The origin of the roughness and porosity of single-layer PFN films has been looked at in the discussion of the pixel fabrication section, where the elastic response of the films to the stress caused from the expansion of the gaseous TP ablation products has been considered. This porosity would act as a barrier to charge transport, and it may also create further gaps between the PFN and the Al, which would act as significant barriers to electron-injection (often the limiting factor in PLEDs²⁸). Despite this rough morphology, functional PLED devices were made using this two-stage LIFT process.

Device Discussion. A wide range of data has been presented here on PFN PLEDs, all with the device architecture ITO/PEDOT:PSS/PVK/PFN/Al. Just looking at the normal LIFTed pixel, it showed impressive device performance, far better than the conventional device on its first run. Strangely, the conventional PFN device improved upon its second run, suggesting that some form of electrical treatment was necessary to initiate good device performance. This could be due to

electrical annealing (i.e., a thermal process) or it could be a mechanical process similar to that observed for the sequentially LIFTed pixels in Figure 9. In addition to these properties, both the normal LIFTed pixel and the conventionally fabricated device had a low breakdown regime: at ~ 18 V and just above 100 mA/cm².

In micrographs of both the normal LIFTed pixel and the conventionally fabricated device (Figures 6c–e and 8), there was evidence of a periodic undulation, confirmed by looking at the donor substrate (see Figure 2) as a spin-coating feature. The main result is the sequential LIFT of a PLED pixel. This is the first time it has been achieved, and despite the high operating voltage, a good EL spectra was obtained and the efficiency was actually higher than the conventionally fabricated device on its first run. A key area for improvement is in the polymer pixel; the single-layer PFN transfer created films with roughnesses of at least $25\text{--}30$ nm when the donor substrate roughness was <3 nm.

In addition to the advantage of transferring otherwise incompatible layers on top of one another, the sequential LIFT process also allows for the transfer of different lateral sizes on top of one another, such as the smaller aluminum pixel on top of the larger PFN pixel in Figure 9. This is advantageous, because it ensures that there are no short circuits between the Al cathode and the ITO anode.

CONCLUSIONS

This work demonstrates that laser-induced forward transfer can be used to sequentially transfer different layers of the same device in individual steps. In addition, it compares pixels fabricated by sequential LIFT with pixels fabricated using normal LIFT (single-step transfer of Al/PFN bilayers) and devices made using conventional fabrication methods. For the sequentially LIFTed pixels, aluminum was LIFTed onto PFN without damaging the underlying layers. The successful application of LIFT to sequentially deposit two functional layers paves the way for the fabrication of more-complex systems with LIFT, with improved device performances. The sequentially LIFTed pixels exhibited functional diode characteristics, with significant light emission.

AUTHOR INFORMATION

Corresponding Author

*E-mail: james.shaw-stewart@ed.ac.uk (J.R.H.S.-S.); thomas.lippert@psi.ch (T.K.L.); frank.nueesch@empa.ch (F.A.N.).

Present Address

[†]Grant Institute, University of Edinburgh, The King's Buildings, Edinburgh EH9 3JW, U.K.

Notes

The authors declare no competing financial interest.

ACKNOWLEDGMENTS

The authors thank Ylenia Maniglio (Empa) for synthesizing the triazene polymer. Financial support is gratefully acknowledged from the FP7 European project e-LIFT (Project 47868—call FP7-ICT-2009-4) and the Swiss National Science Foundation.

REFERENCES

- (1) Tang, C. W.; Van Slyke, S. A. *Appl. Phys. Lett.* **1987**, *51*, 913–915.
- (2) Bohandy, J.; Kim, B. F.; Adrian, F. J. *J. Appl. Phys.* **1986**, *60*, 1538–1539.
- (3) Arnold, C.; Serra, P.; Piqué, A. *MRS Bull.* **2007**, *32*, 23–31.

- (4) Tolbert, W. A.; Sandy Lee, I.-Y.; Doxatader, M. M.; Ellis, E. W.; Dlott, D. D. *J. Imaging Sci. Technol.* **1993**, *37*, 411–421.
- (5) Doraiswamy, A.; Narayan, R.; Lippert, T.; Urech, L.; Wokaun, A.; Nagel, M.; Hopp, B.; Dinescu, M.; Modi, R.; Auyeung, R.; Chrisey, D. *Appl. Surf. Sci.* **2006**, *252*, 4743–4747.
- (6) Xu, J.; Liu, J.; Cui, D.; Gerhold, M.; Wang, A. Y.; Nagel, M.; Lippert, T. K. *Nanotechnology* **2007**, *18*, 025403.
- (7) Rapp, L.; Cibert, C.; Nénon, S.; Alloncle, A. P.; Nagel, M.; Lippert, T.; Videlot-Ackermann, C.; Fages, E.; Delaporte, P. *Appl. Surf. Sci.* **2011**, *257*, 5245–5249.
- (8) Banks, D. P.; Kaur, K.; Gazia, R.; Fardel, R.; Nagel, M.; Lippert, T.; Eason, R. W. *Europhys. Lett.* **2008**, *83*, 38003.
- (9) Palla-Papavlu, A.; Dinca, V.; Paraico, I.; Moldovan, A.; Shaw-Stewart, J.; Schneider, C. W.; Kovacs, E.; Lippert, T.; Dinescu, M. *J. Appl. Phys.* **2010**, *108*, 033111–6.
- (10) Dinca, V.; Palla-Papavlu, A.; Dinescu, M.; Shaw-Stewart, J.; Lippert, T.; Di Pietrantonio, F.; Cannata, D.; Benetti, M.; Verona, E. *J. Appl. Phys. A: Mater. Sci. Process.* **2010**, *101*, 559–565.
- (11) Palla-Papavlu, A.; Paraico, I.; Shaw-Stewart, J.; Dinca, V.; Savopol, T.; Kovacs, E.; Lippert, T.; Wokaun, A.; Dinescu, M. *J. Appl. Phys. A: Mater. Sci. Process.* **2011**, *102*, 651–659.
- (12) Fardel, R.; Nagel, M.; Nuesch, F.; Lippert, T.; Wokaun, A. *J. Appl. Phys. Lett.* **2007**, *97*, 061103.
- (13) Kattamis, N. T.; McDaniel, N. D.; Bernhard, S.; Arnold, C. B. *Org. Electron.* **2011**, *12*, 1152–1158.
- (14) Shaw-Stewart, J.; Lippert, T.; Nagel, M.; Nüesch, F.; Wokaun, A. *ACS Appl. Mater. Interfaces* **2011**, *3*, 309–316.
- (15) Shaw Stewart, J.; Lippert, T.; Nagel, M.; Nüesch, F.; Wokaun, A. *J. Appl. Phys. Lett.* **2012**, *100*, 203303–4.
- (16) Huang, F.; Wu, H.; Wang, D.; Yang, W.; Cao, Y. *Chem. Mater.* **2004**, *16*, 708–716.
- (17) Shaw Stewart, J.; Chu, B.; Lippert, T.; Maniglio, Y.; Nagel, M.; Nüesch, F.; Wokaun, A. *J. Appl. Phys. A: Mater. Sci. Process.* **2011**, *105*, 713–722.
- (18) Wu, H.; Huang, F.; Peng, J.; Cao, Y. *Synth. Met.* **2005**, *153*, 197–200.
- (19) Chen, Z.; Niu, Q.; Zhang, Y.; Ying, L.; Peng, J.; Cao, Y. *ACS Appl. Mater. Interfaces* **2009**, *1*, 2785–2788.
- (20) Nagel, M.; Hany, R.; Lippert, T.; Molberg, M.; Nüesch, F. A.; Rentsch, D. *Macromol. Chem. Phys.* **2007**, *208*, 277–286.
- (21) Müller-Buschbaum, P.; Gutmann, J.; Kraus, J.; Walter, H.; Stamm, M. *Macromolecules* **2000**, *33*, 569–576.
- (22) Fardel, R.; Feurer, P.; Lippert, T.; Nagel, M.; Nüesch, F. A.; Wokaun, A. *J. Appl. Surf. Sci.* **2007**, *254*, 1332–1337.
- (23) Nagel, M.; Fardel, R.; Feurer, P.; Häberli, M.; Nüesch, F.; Lippert, T.; Wokaun, A. *J. Appl. Phys. A: Mater. Sci. Process.* **2008**, *92*, 781–789.
- (24) Fardel, R.; Nagel, M.; Nüesch, F.; Lippert, T.; Wokaun, A. *J. Appl. Surf. Sci.* **2009**, *255*, 5430–5434.
- (25) Fardel, R.; Nagel, M.; Nüesch, F.; Lippert, T.; Wokaun, A. *J. Appl. Surf. Sci.* **2007**, *254*, 1322–1326.
- (26) Lippert, T.; Nakamura, T.; Niino, H.; Yabe, A. *Macromolecules* **1996**, *29*, 6301–6309.
- (27) Fardel, R.; Nagel, M.; Nüesch, F.; Lippert, T.; Wokaun, A. *J. Phys. Chem. C* **2010**, *114*, 5617–5636.
- (28) Parker, I. D. *J. Appl. Phys.* **1994**, *75*, 1656–1666.